Available online at www.sciencedirect.com
SCIENCE DIRECT®
Journal of Molecular Graphics and Modelling 23 (2004) 39–49
Journal of Molecular Graphics and Modelling
www.elsevier.com/locate/JMGM

Comparative modeling of a GABAA alpha1 receptor using three crystal structures as templates

J.R. Trudell *, E. Bertaccini [1]

Department of Anesthesia and Beckman Program for Molecular and Genetic Medicine, Stanford University, Stanford, CA 94305-5117, USA

Received 3 October 2003; received in revised form 20 February 2004; accepted 3 March 2004
Available online 17 April 2004

Abstract

We built a model of a GABAA alpha1 receptor (GABAAR) that combines the ligand binding (LBD) and the transmembrane domains (TMD). We used six steps: (1) a four-alpha helical bundle in the crystal structure of bovine cytochrome *c* oxidase (2OCC) was identified as a template for the TMD of a single subunit. (2) The five pore-forming alpha helices of a bacterial mechanosensitive channel (1MSL) served as a template for the pentameric ion channel. (3) Five copies of the tetrameric template from 2OCC were superimposed on 1MSL to produce a homopentamer containing 20 alpha helices arranged around a funnel-shaped central pore. (4) Five copies of the GABAAR sequence were threaded onto the alpha-helical segments of this template and inter-helical loops were generated to produce the TMD model. (5) A model of the LBD was built by threading the aligned sequence of GABAAR onto the crystal structure of the acetylcholine binding protein (1I9B). (6) The models of the LBD and the TMD were aligned along a common five-fold axis, moved together along that axis until in vdW contact, merged, and then optimized with restrained molecular dynamics. Our model corresponds closely with recently published coordinates of the acetylcholine receptor (1OED) but also explains additional features. Our model reveals structures of loops that were not visible in the cryoelectron micrograph and satisfies most labeling and mutagenesis data. It also suggests mechanisms for ligand binding transduction, ion selectivity, and anesthetic binding.

Keywords: Molecular modelling; Anesthetics; Molecular dynamics; Ligand-gated ion channels; Alpha helices; Helical bundles

1. Introduction

The Cys-loop superfamily of ligand-gated ion channels (LGICs) includes nicotinic acetylcholine (nAChR), GABAAR, glycine (GlyR), and 5-hydroxytryptamine (5HT3) receptors [1–6]. Most studies of these receptors, using site-directed mutagenesis and chemical labeling techniques, have focused on either the ligand-binding domain (LBD) or the transmembrane domain (TMD). More recently, however, it has become clear that a description of the interaction between these domains will be necessary to understand how agonists activate the ion channels [7] as well as how anesthetics and alcohols may alter this process [1,8,9]. Fortunately, preparation of a comparative model that combines both domains has been made possible by the recent publication of high-resolution crystal structures of proteins that can serve as templates for both domains. Here we describe building a model of the TMD by using the structure of a pentameric ion channel to align five copies of a four-alpha helical bundle. We then merged the TMD model with our previously published model [10] of the LBD that was built by threading the sequence of GABAAR onto the crystal structure of an acetylcholine binding protein (AChBP) from the snail *Lymnaea stagnalis* [11]. Despite being derived using a completely different technique, much of our model agrees with the overall form of the recently published model of the homologous torpedo nAChR that was derived by aligning four polyalanine alpha helices onto the electron density of a 4 A resolution cryoelectron micrograph [12]. The additional value of our model comes from illustration of features not visible in the nAChR model at its

* Corresponding author. Tel.: +1-650-7255839; fax: +1-650-7258052.
E-mail address: trudell@stanford.edu (J.R. Trudell).
[1] Present address: Palo Alto Veterans Affairs Health Care System, Palo Alto, CA 94304, USA.

1093-3263/$ – see front matter © 2004 Elsevier Inc. All rights reserved.
doi:10.1016/j.jmgm.2004.03.004

present moderate resolution, especially the loops that connect alpha helices in the TMD with loops in the LBD. In addition, our model successfully incorporates and explains a large body of information derived from site-directed mutagenesis, photoaffinity labeling, as well as anesthetic and alcohol binding. Our model of GABAAR will allow comparison with the overall morphology of nAChR deduced by cryoelectron microscopy. In particular, it will be possible to compare modes of anion-conductance in GABAAR and GlyR with cation-conductance in nAChR. This model will also serve as a platform from which future site-directed mutagenesis studies can be planned and theories of anesthetic action tested.

2. Methods

We built our model in six steps: (1) a four-alpha helical bundle found in the crystal structure of bovine cytochrome *c* oxidase (2OCC) [13] was identified as a template for the TMD of a single subunit. (2) The five pore-forming alpha helices of a bacterial mechanosensitive channel (1MSL) were used as a template for the pentameric ion channel of GABAAR (PDB entry 1MSL) [14]. (3) Five copies of the tetrameric subunit were packed according to a partial alignment with the pentameric template to produce a homopentamer containing 20 alpha helices arranged around a central pore in the shape of a funnel that opens toward the extracellular side. (4) Five copies of the aligned sequence of GABAAR were threaded onto the alpha-helical segments of this template and inter-helical loops were generated with the Insight II (v 2000.1) suite of programs (Accelrys, San Diego, CA) on an Octane workstation (SGI, Mountain View, CA). (5) A model of the ligand-binding domain was built by threading the aligned sequence of GABAARa1 onto the crystal structure of the acetylcholine binding protein from *Lymnaea stagnalis* (1I9B) [11]. (6) The two models were aligned along a common five-fold axis, moved together along that axis until in vdW contact, merged, and then optimized with restrained molecular dynamics in Insight II.

2.1. Finding a template for the four-helical bundle domain

It has long been clear that the TMD of LGICs contains four hydrophobic segments of about 20 amino acid residues each [2,3,15]. However, it has been controversial whether these segments are alpha helices, beta strands, or a mixture of motifs. We recently used a consensus of 10 secondary structure prediction methods to show that all four segments are alpha helical [16]. This prediction is in agreement with recent experimental data [17] and with the most recent interpretation of cryoelectron micrographs of the nAChR [12]. The short loops connecting the first three of the transmembrane alpha helices dictated the anti-parallel arrangement of alpha helices found in four-helical bundles. As a result, we searched for four-helical bundles that would be suitable as templates for our model of GABAAR.

We have discussed the selection of this template previously [1,18]. Briefly, the amino acid sequence of the human GABAA alpha1 was edited to remove the precursor sequence and residues in the TM3–TM4 loop. The program, SeqFold [19], was used to search a sequence database of 3D proteins that was based on the Brookhaven protein database. This process consistently returned the ''hit'' of the structure abbreviated as 2CCY, a heme-containing tetrameric bundle of alpha helices [13]. Using the most recent version of the CATH database of proteins categorized based on fold type, 2CCY was then used as input to the VAST search engine [20] in order to focus a more refined search. Subdomain 2 of chain C within the bovine cytochrome c oxidase structure 2OCC.pdb [13] was located within this focused database of tetrameric alpha-helical bundles. The PDB file for 2OCC was edited so that it contained only the four-helical bundle being considered. (Hereafter we refer to subdomain 2 of chain C in cytochrome *c* oxidase as 2OCC-4H.)

2.2. Finding a template for the pentameric ion pore

The global structure of the superfamily of ligand-gated ion channels, as exemplified in nAChR, was revealed by cryoelectron microscopy to consist of five subunits arranged around a five-fold axis, each subunit consisting of three domains; an extracellular LBD, a transmembrane TMD, and an intracellular domain [12,21–23]. The pore-lining helices of the nAChR TMD have been modeled previously as a pentamer of alpha helices by imposing a series of intra-helix, inter-helix, and inter-residue distance restraints [24,25]. The five pore-lining helices have also been modeled as essentially parallel bundles of alpha helices without imposing such restraints [26–28].

However, there is much evidence that the ion pore admits large molecules only from the extracellular side and that depth of penetration into the pore is a function of molecular size [2,3,6,29–34]. As a result, it seems clear that the pore must be shaped like a funnel that opens toward the extracellular side (Fig. 1A). Indeed, this motif was found in the crystal structure of MscL, a bacterial mechanosensitive ion channel (PDB entry 1MSL) [35]. This structure has been suggested to be a progenitor of pentameric ion channels [30]. We previously used the five pore-lining alpha helices in this structure as a template for aligning the pore-lining transmembrane segment 2 (TM2) in models of GABAAR, GlyR, and nAChR ion channels [1,6–8,18,32]. The MscL structure also contains five outer alpha helices that contribute to the ion channel only as the funnel-shaped pore widens outward on the extracellular side. In our previous models, we considered these outer helices to take the part of TM1 in GABAAR.

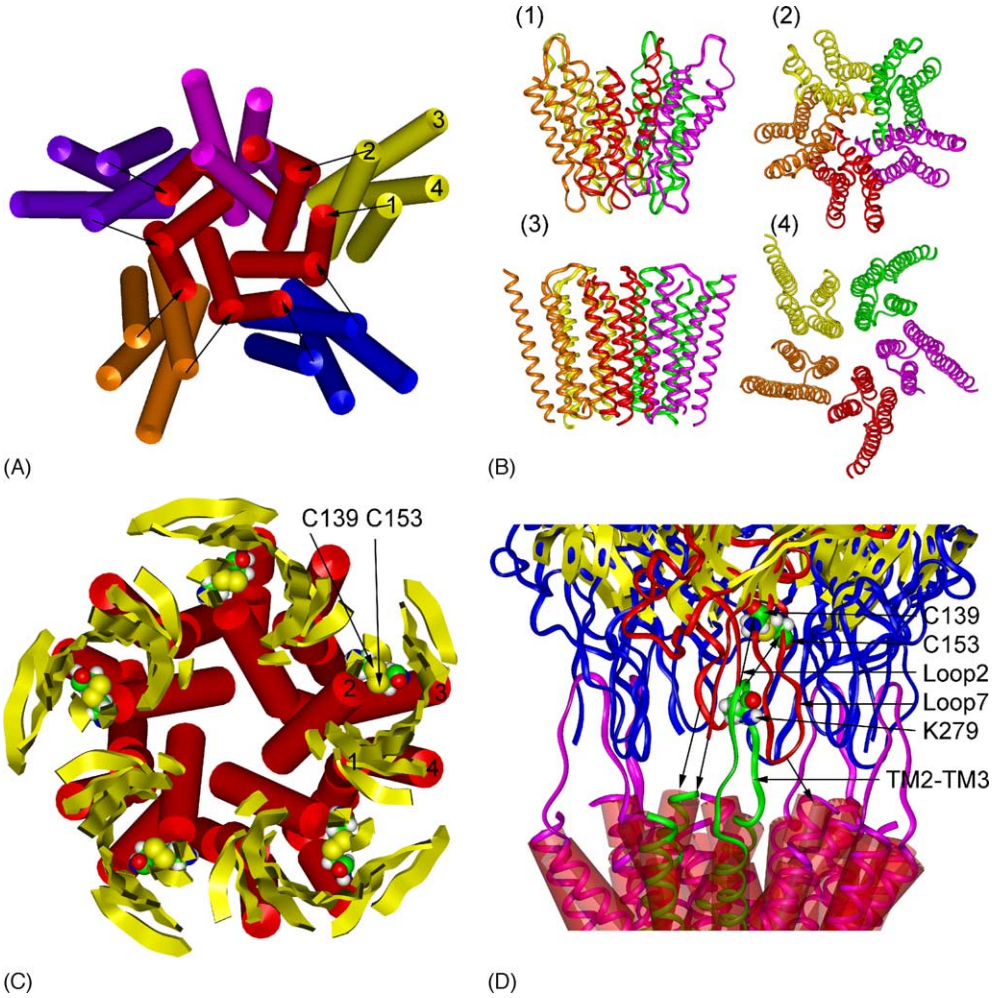

Fig. 1. (A) Assembly of five copies of 2OCC-4H onto the inner and outer pore helices of 1MSL (red cylinders). Arrows indicate motions of 15 A radially inward toward the central axis. One copy of 2OCC-4H (yellow helices) is labeled with numbers of TMD segments. One copy of 2OCC-4H (violet helices, top) is in the final position to show the good overlap between helices 1 and 2 in the two templates. (B) The 20 alpha helices in the present model (B1, side view and B2 view from extracellular side) compared with the model based on the cryoelectron micrograph of nAChR 1OED (B3, side view and B4 view from extracellular side). The five subunits are shown in individual colors. (C) A view down the five-fold axis from the extracellular side. Top and bottom clipping planes isolate the interface between the LBD and TMD. Two criteria are illustrated: (1) the two cysteine residues of the LBD "Cys-loop" (Cys139 and Cys153) should be over the alpha helices (red cylinders) of the TMD; (2) the beta sheets (yellow ribbons) of the LBD should be positioned over the TMD. (D) A view from the side of the receptor, at the interface of the LBD and TMD. Distance restraints (black arrows) were applied to pull loops 2 and 7 of the LB domain gently toward the TM domain while similar restraints extended the TM2–TM3 loop toward the LB domain. Iteratively, the TM domain was moved upward 2.5 A, the distance restraints were shortened by 2.5 A, and the assembly was re-optimized.

2.3. Superimposing five copies of 2OCC-4H onto the 1MSL ion pore template to create a 20-alpha-helical template

The PDB file for the bacterial mechanosensitive ion channel (1MSL) was edited so that it contained only the five inner and outer helices that define the TMD ion channel (A10–A40). The goal was to superimpose the second helix of 2OCC-4H (corresponding to TM2 of LGICs) such that residues know to face the ion pore (2′, 6′, 9′, 10′, 13′ in nAChR notation) were appropriately oriented (Fig. 1A). The heptad arrangement of an alpha helix allowed this restraint to be met by only two such superpositions on 1MSL and both were tested. Residues were aligned such that (1) backbone atoms of residues C160–C170 of the second alpha-helical segment of 2OCC-4H were superimposed on residues A24–A34 of the inner pore-lining helices of 1MSL; (2) backbone atoms of residues C167–C177 of the second alpha-helical segment of 2OCC-4H were superimposed on residues A24–A34 of 1MSL. Both alignments were tested by threading the GABAAR sequence as described below.

2.4. Threading GABAAR onto the 20-alpha-helical template

The primary sequence of the human GABAAR was edited to make a TMD sequence beginning at Tyr225 and ending at Asn417. The long intracellular loop connecting TM3 and TM4 was replaced by six glycine residues. This loop segment was chosen because connecting loops with

more than five glycine residues do not alter the transition state of folding/refolding in the helical bundle of Rop [36] and a molecular dynamics simulation determined that seven glycine residues were optimum for a helix-loop-helix motif [37].

Previous experience suggested that it is best to thread the four predicted alpha-helical segments of GABAAR separately onto the corresponding alpha-helical segments in the template of a four-helical bundle [8]. Therefore, the edited sequence of GABAAR was divided into four predicted alpha-helical segments: Ile228–Asn248, Ala254–Ser276, Ala285–Asn308, and Arg394–Asn417. These segments were aligned with the four alpha-helical segments in 2OCC-4H; C129–C149, C161–C183, C195–C218, C235–C258. The initial alignment was based upon the aforementioned SeqFold analysis. We then generated the three interconnecting loops using the Homology module of Insight II. The resulting model of the TMD (Fig. 1B) corresponds closely to the coordinates in the homologous nAChR (1OED) [12].

2.5. Constraints used for threading GABAAR onto the templates

Here we review the key constraints that we used to refine the threading of each segment of GABAAR. This study is comparative modeling, rather than homology modeling, because a large amount of labeling and mutagenesis data helped to restrain the TMD model, whereas the sequence homology of GABAAR with the templates is low.

TM1 is known to form part of the ion channel as the funnel shape of the pore widens toward the extracellular side [2,22,30,38]. Water-soluble reagents label several TM1 residues N-terminal to a conserved Pro233 [39]. As discussed below, the top of TM1 forms the only covalent attachment to the ligand-binding domain and we expected, but did not constrain, that the functionally important Gly224 [40] in our model should be near the C-terminal residue in the model of the ligand-binding domain based on AChBP. In addition, residues corresponding to Leu232 have been found to modulate potentiation of GABA activation by anesthetics and this position may face toward the center of the four-alpha helical bundle [18,41].

TM2 is the alpha helix that contributes the pore-forming residues in each subunit. It has been extensively studied by site-directed mutagenesis [2,3,33,42] and photolabeling [6,38]. We tried to combine data from all members of the "Cys-loop" superfamily in constraining our model. However, we did so with caution because there is evidence that, in the heteromeric nAChR, the alpha subunits move both to a greater degree and independently from the other subunits [22]. The residues most exposed to the pore in the resting state correspond to GABAAR Val257 (2′), Thr261 (6′), Leu264 (9′), Thr265 (10′), and Thr268 (13′) (in shorthand notation where 1′ = Thr256) [3,6,42]. In contrast, site-directed mutation of Ser270 (15′) has large effects on potentiation of GABA activation by anesthetics. It is likely that this position faces toward the center of the four-alpha helical bundle [18,41,43–45].

TM3 is not labeled by water-soluble reagents in the ion pore and it is only slightly accessible to reagents thought to be at the lipid–protein interface [15]. As a result, it is likely to be in an inter-subunit location. However, recent studies have shown that residues on TM3 can be labeled by reagents that presumably enter a water-filled cavity in the center of the subunit [45,46]. In addition, site-directed mutation of Ala291 affects potentiation of GABA activation by anesthetics and it is likely that this position faces toward the center of the four-alpha helical bundle [18,41,43]. An additional constraint is that the volume of side chains substituted for Val285 of the nAChR correlates with activation by acetylcholine (corresponding to Val297 in GABAAR), suggesting that this residue also faces into the center of the subunit [47].

The TM3–TM4 loop is approximately 100 residues long and is thought to contribute regulatory sites to the receptors [2]. It is likely that it forms the cytoplasmic vestibule imaged by cryoelectron microscopy [21]. There is recent evidence that it is involved in clustering during receptor expression in the membrane [23]. However, there is little structural information available about this domain and we have substituted it with a short inter-helical loop.

TM4 is likely to be exposed to the lipid bilayer as it is labeled by a variety of hydrophobic reagents [15,38] and cholesterol analogs [48,49]. This segment has the lowest homology within the "Cys-loop" superfamily of LGICs and it was demonstrated that substituting the native segment with an irrelevant chimera could form functional nAChRs [50]. On the other hand, recent site-directed mutations, in particular two tryptophan-scanning studies, have shown that individual residues have important effects on ion channel gating and potentiation of agonists by anesthetics [51,52]. A particularly interesting residue is Tyr411 in GABAAR where substitution by tryptophan changes the GABA ED50 [52]. The corresponding Thr422 in nAChR can only be replaced with residues capable of hydrogen bonding or function will be lost [53]. This same residue is a target for hydrocortisone binding [54]. Threading of TM4 was also guided by substitution tables for alpha-helical TMD proteins that show that Cys, Asn, Pro, Gln, and Tyr are rarely lipid facing [55].

2.6. Inter-helical loops and coordinate assignments

Three inter-helical loops were generated with the Homology module of Insight II 2000. This process was repeated four times until all residues in five copies of GABAAR had backbone coordinates assigned. The five subunits were merged into a single molecule so that the autorotamer and "bump check" functions would check for inter-subunit contacts as well as intra-subunit steric overlaps. We set all charged residues to pH = 7, assigned

potentials with the CFF91 force field, tethered all backbone atoms to their initial positions with a quadratic force constant of 100 kcal/A2, optimized the model with the Discover_3 module to a derivative of 1 kcal/A, relaxed it with 5000 steps (1 fs) of constrained molecular dynamics [56,57] at 400 K, and then re-optimized it to a derivative of 1 kcal/A. We used a dielectric = 4 and the default atom-based Coulombic interactions in Insight II (cutoff distance of 9.5, 1 A spline width, 0.5 A buffer) and used steepest descent followed by Polak–Ribiere conjugate gradient minimization.

2.7. Selecting the best alignment of four-helical bundles on 1MSL

As described above, we tested two possible alignments of 2OCC-4H onto 1MSL: backbone atoms of either residues C160–C170 or residues C167–C177 of the second alpha-helical segment of 2OCC-4H were superimposed on residues A24–A34 of the inner pore-lining helices of 1MSL. We tested the two resulting models of the TMD by comparing dimensions of the resulting ion pore with experimental results [2,3,15,32]. The alignment of residues C167–C177 of 2OCC-4H with residues A24–A34 of 1MSL produced the best fit and this TMD model was used to merge with the LBD as described below.

2.8. Threading GABAAR onto the template for the ligand-binding domain

We have previously published construction of the extracellular ligand-binding domain of the GABAAR by threading the primary sequence of GABAAR onto the crystal structure of the AChBP [10]. Briefly, 212 residues in the primary sequence of GABAAR were aligned with AChBP (five C-terminal residues not in PDB file were modeled as a beta strand) and backbone coordinates were assigned with the exception of loops 2 and 7 in the AChBP structure. The latter loops have no function in the structure of water-soluble AChBP and they are collapsed against the protein. In contrast, in LGICs it is likely that they intercalate with the TM2–TM3 loop [7,12,22,58]. Therefore, 10 possible conformations of each loop were generated with the Homology module, the most extended loops were selected, and two identical loops were replicated in all five subunits. The five subunits were merged into a single molecule so that the autorotamer and ‘‘bump check’’ functions would check for inter-subunit contacts as well as intra-subunit steric overlaps. We optimized the model as described for the TMD.

2.9. Merging LBD and TMD models

We have recently described coupling between residues in the TM2–TM3 loop and residues in loops 2 and 7 in the LBD [7]. A model was built in which the TM2–TM3 loop (containing a positive charge on Lys279) arched upward toward the LBD while loops 2 and 7 (each containing two negatively charged residues) arched downward on either side of the TM2–TM3 loop. This model explained the success of double charge exchange mutations as well as disulfide cross-linking experiments [7]. This structural motif of three intercalating loops was used in merging the two domains in the present model. A previous model built by Unwin et al. was of particular value when we combined the LBD with the TMD, because they aligned their model of the LBD with the electron density of a cryoelectron micrograph [22]. This alignment showed that the sulfur atoms of the two cysteine residues that define the ‘‘Cys-loop’’ are directly above a ‘‘rod of electron density’’ in each subunit (Fig. 1C).

Our general approach was to align both models along a common five-fold symmetry axis and move them together with the following constraints: (1) Rotation of the ligand-binding domain about the five-fold axis should place the sulfur atoms of the two highly conserved cysteine residues that define the ‘‘Cys-loop’’ over the top of the TM2 [22]. (2) Movement of the ligand-binding domain toward the TMD along the five-fold axis should allow the TM2–TM3 loop (Leu277–Asp287) to intercalate between loops 2 (Pro52–Ile62) and 7 (Cys139–Cys153) in the ligand-binding model [7]. It was straightforward to align the two models on a common five-fold axis and rotate one model until the sulfur atoms were in the desired position (Fig. 1C).

In contrast, motion along the five-fold axis proceeded carefully in small steps to avoid adverse vdW contacts that would distort the combined models during an optimization. Many preliminary attempts resulted in the following procedure (Fig. 1D): The TMD model was moved toward the ligand-binding model until the extended C-terminus of the LBD was 12A from the N-terminus of the TMD. Two distance restraints were used to hold the TM2–TM3 loop between loops 2 and 7 without twisting. Quadratic distance restraints (20 A, force constant 100 kcal/A2) were assigned between the Ca atoms of residues Val280 and Ala281 in the TM2–TM3 loop and the Ca atoms of Cys139 and Cys153 in loop 7, respectively. Loops 2 and 7 were extended downward toward the TMD by setting 20 A distance restraints between the Ca atoms of Asp57 in loop 2 (LBD) and Tyr225 at the top of TM1 (TMD) as well as between the Ca atoms of Asp145 in loop 7 (LBD) and Tyr225 at the top of TM1 (TMD) in the adjacent subunit (counterclockwise as viewed from the extracellular side). In order to satisfy our experimental data regarding Coulombic interactions between Lys279 and both Asp57 and Asp149 [7], flat-bottomed distance restraints were set between the sidechain N (NH3) atoms of Lys279 and the sidechain C (CO2) atoms of the two aspartate residues (no penalty between 2 and 5 A, 100 kcal/A2 elsewhere). We fixed the position of all backbone atoms in both models with the exception of those in loops 2, 7, TM1–TM2, TM2–TM3, and TM3–TM4 and then optimized the assembly of the two models with the parameters described above for the TMD model. This optimization had the desired

result of both extending the three loops and ensuring that they intercalated as they approached, in agreement with our experimental data [7]. This process was repeated by moving the TMD model toward the LBD model by 2.5 A along the five-fold axis, decreasing the distance restraints on the loops by 2.5 A, and re-optimizing with the same parameters.

When the LBD and TMD domains were in vdW contact, the distance restraints between the LBD C-terminus and the TMD N-terminus were removed and an amide bond was formed. Backbone restraints were removed from the last five C-terminal residues of the ligand-binding model to allow flexibility near the new amide bond, and the assembly was re-optimized. Then the model was relaxed with 10,000 fs (1 fs steps) of constrained molecular dynamics at 400 K [56] and re-optimized to a derivative of 1 kcal/A. Finally, backbone restraints were maintained on the LBD (since it was derived from a crystal structure) but removed from the TMD model, and the assembly was re-optimized to a derivative of 1 kcal/A. This unrestrained optimization of the TMD was a test of the stability of the combined structure.

3. Results

3.1. Geometry and dimensions

The overall dimensions of the combined model (Fig. 2A and B) approximate the electron density envelope in the

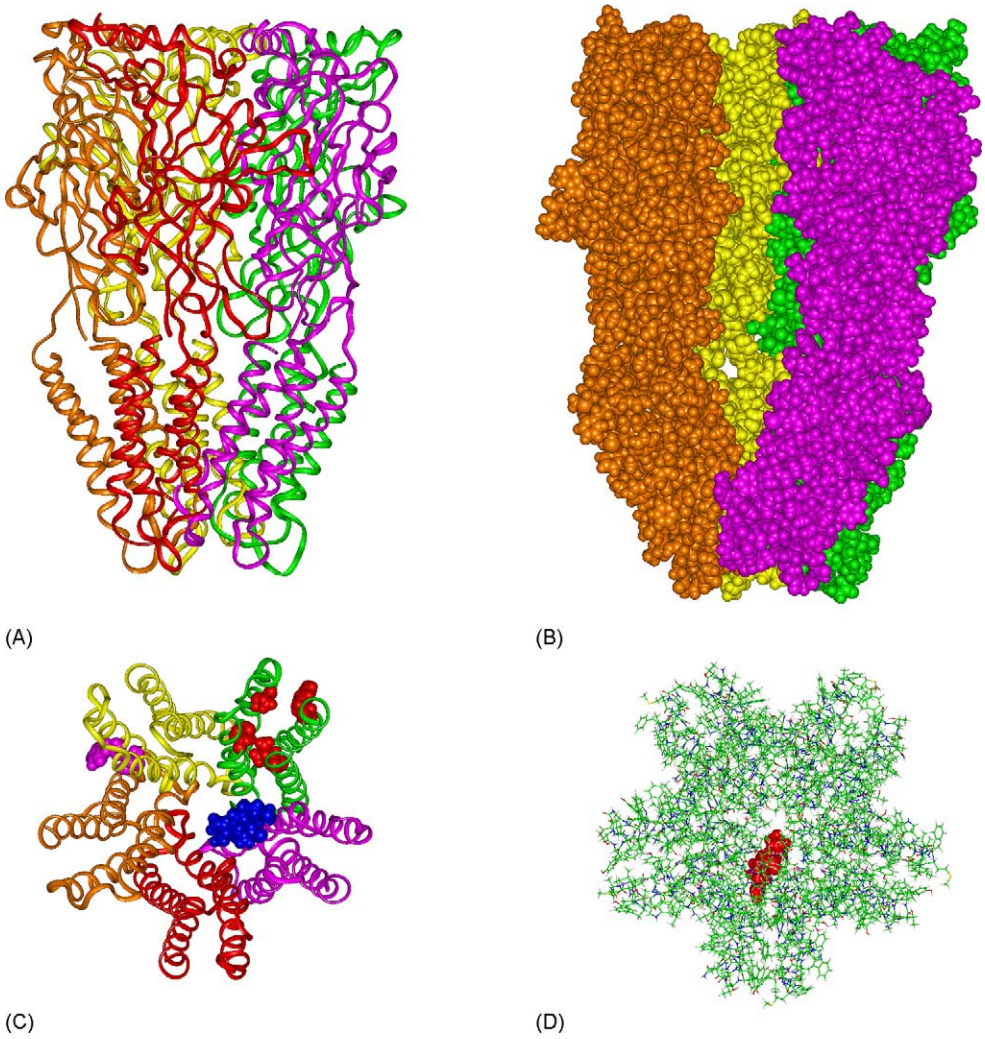

Fig. 2. (A) A view from the side of the receptor in the plane of the membrane. The right-hand twist of the model and the tight inter-subunit interactions are evident. The foreground subunit is rendered with a red ribbon and other subunits are colored as in Fig. 1. (B) A view of the side of the receptor from the center of the ion pore. The foreground subunit (red ribbon in (A)) was deleted to reveal the interior of the ion pore (subunits colored as in Fig. 1). (C) A view down the five-fold axis of the TMD from the extracellular side. The amino acid backbone of each subunit is rendered as a ribbon, colored as in Fig. 1. In one subunit (pink ribbon), residues labeled with hydrophilic reagents are rendered with space-filling blue surfaces (in prime notation: 2′, 6′, 9′, 10′, and 13′). In a second subunit (green ribbon), residues proposed to provide an anesthetic binding site are red (L232, S270, A291, Y411). In a third subunit (yellow ribbon), residues that react with hydrophobic reagents are pink (F296 and S299). (D) A view down the five-fold axis of the TMD from the extracellular side. Amino acid residues are rendered with stick features. In one subunit, residues thought to be involved in gating are rendered as space-filling surfaces and colored red (P253, A254, R255). The overall dimensions approximate the electron density envelope in the cryoelectron micrograph of torpedo nAChR.

cryoelectron micrographs of nAChR [12,21,22]. In addition, there was a smooth transition between the end of the ion pore of the TMD and the beginning of the pore in the LBD (Fig. 2B). The C-terminal residue of the LBD made an amide bond with the N-terminal of the TMD with very little stretching or distortion of the structure (Fig. 2B). Globally, it appears that the comparative model of the TMD intercalates very well with the LBD model based on the crystal structure of the AChBP [11]. In addition, the backbone atoms of the entire complex both before and after an unconstrained optimization (13,024 atoms) could be superimposed with an RMS of 0.27 A. The size of the pore tapered from 25 A on the extracellular side to 3 A on the intracellular side. The location of residues known to be involved in ion selectivity [59–61] are appropriately located in the TM1-2 loop (Fig. 2A). The combination of the right-twisted funnel shape of the ion pore and the intervention of TM1 at the extracellular end of the ion pore allowed a tight channel to be formed. The pore is therefore lined by residues from both TM1 and TM2 (Fig. 2C and D).

3.2. Localization of an anesthetic binding pocket

Four residues known to be involved in anesthetic and alcohol effects are located within the core of each transmembrane tetramer. These include GABAAR Leu232, Ser270, Ala291 and Tyr 411 [1,41,43,52]. They occur at approximately the same vertical level in each alpha helix, thereby converging on a pocket-like region on the extracellular side of the narrowest point formed by the left-handed crossing of the four helices (Fig. 2A and C).

3.3. Fit with experimental studies

TM1 forms part of the extracellular ion pore and would be exposed to labeling by water-soluble reagents in the pore in agreement with experimental data [39] (Fig. 2C and D). A point that is not obvious from looking at models of only the TMD is that the covalent linkage to the C-terminal residue of the LBD pulls TM1 slightly away from TM2 and increases exposure of the top of TM1 (Fig. 2A). This feature may explain the functional importance of the C-terminal Gly224 in receptor function [40]. The highly conserved Pro233 one third of the way down TM1 is well positioned to adapt the top of TM1 to the role of a pore-lining segment [62], as it occurs in the region where TM1 crosses TM2 and begins to contribute to the expanding funnel shape of the ion pore (Fig. 2A). TM2 is the major alpha helix in the ion channel and residues that are labeled in the resting state are suitably exposed to the pore [2,3,6,33,38,42] (Fig. 2C and D). Although we previously predicted TM2 to end at Arg274 [16], the present model (Fig. 2A) supports recent data that it extends as an alpha helix to at least Pro278 [58]. The residue most important for modulation of GABA potentiation by anesthetics and alcohols (Ser270) [43,45] faces inward toward the center of the subunit (Fig. 2A and C). The center of each subunit forms a cavity that is known to be water-filled and that allows penetration by both neutral [45] and charged methanethiosulfonate reagents [46].

The TM2–TM3 loop intercalates between loops 2 and 7 of the ligand-binding model [7]. Of course, this was initially a constraint in building the model. Nevertheless, it remained stable after final unrestrained optimization. It is apparent that it provides a possible coupling between the postulated movement of the two beta sheet regions connected to loops 2 and 7 [11,22,63] and movement of the TMD helices in a subunit. Negatively charged residues from loops 2 and 7 [7] surround the positively charged Lys279 in the TM2–TM3 loop. Our collaborators tested the proximity of residues suggested by our model by performing charge-exchange mutations and disulfide cross-linking experiments in GABAAR subunits expressed in HEK cells. In GABAAR alpha1 subunits single charge exchange mutations (K279D in the TM2–TM3 loop or D149K in loop 2 of the LBD) dramatically impaired gating and raised the GABA ED50. Proximity of these residues was demonstrated by rescue of gating with a double charge-exchange mutation (K279D/D149K). Moreover, proximity of the same residues was confirmed by forming a disulfide link between a double cysteine mutation (K279C/D149C) [7]. We then used our present model as a template to build a model of a GABAAR beta 2 by threading the beta 2 sequence on it and building in loops as required. This model of beta 2 predicted different residues would be in proximity. Our collaborators again confirmed this prediction with charge-exchange and disulfide cross-linking experiments [64]. These results suggest the possibility that interactions of loops in the LBD and TMD are part of the transduction of ligand binding energy to the ion channel gate.

During the optimization and dynamics steps, an interesting salt bridge formed between Arg274 and Asp287 in this model (both residues are near the extracellular ends of TM2 and TM3, respectively). Its role is unclear, as these residues are not conserved in the nAChR family. However, it may serve to orient TM2 and TM3 or to act as a hinge between them. Mutation of Arg274 to Ala results in an approximately 30-fold right shift of the GABA EC50 [65].

TM3 is not exposed to the ion pore and is only partially exposed to the lipid bilayer, consistent with labeling data [15] (Fig. 2C). One face of TM3 is positioned for labeling by reagents that could enter a water-filled cavity at the center of the subunit [46]. The side-chain volume of site-directed mutations of Val285 in nAChR (corresponding to Val297 in GABAAR) correlates with gating activity and this residue is therefore thought to be buried in the center of the subunit [47]; this residue does face inward in the model. A residue important for modulation of GABA potentiation by anesthetics and alcohols (Ala291, Fig. 2A) [41,43] correctly faces toward the center of the subunit and the putative water-filled cavity. As described in Section 2, the TM3–TM4 loop was truncated and modeled as a short extended loop of six glycine residues. This intracellular domain is thought to

regulate ion channel function, but its structure and function have received less attention [2]. For our present purposes, it is sufficient that the loop neither produced steric overlaps with neighboring subunits nor distorted TM3 and TM4 [36,37].

TM4 was the most difficult to model because of low homology among members of the ''Cys-loop'' superfamily. Its construction was also challenging because of somewhat contradictory results between labeling with hydrophobic labels [15,66], labeling with cholesterol analogs [48], interactions with anesthetic steroids [49], and results of site-directed mutagenesis studies [51–53]. Fortunately, side chain packing interactions in bovine cytochrome c oxidase, our template for a four-helical bundle, have been studied carefully [13,67]. Moreover, a study of known side chain conformations in crystal structures of other alpha-helical bundles has revealed a surprising propensity for residues normally associated with external positions to be buried within bundles, for example tyrosine and tryptophan residues [55]. We observed that our template, 2OCC-4H, had tyrosine and tryptophan residues buried at either inter-helical or central sites in the four-helical bundle. Therefore, we accepted an alignment of TM4 with 2OCC-4H that placed residues that are labeled with hydrophobic reagents at inter-helical sites (Fig. 2A and B). We also reasoned that regions at the interface between two alpha helices and the lipid bilayer might be ideal binding sites for hydrophobic reagents as well as cholesterol and cholesterol analogs.

4. Discussion

Our model of a GABAAR was constructed using homology modeling based on the three templates. It was further refined using a variety of experimental results as initial constraints. However, even with restraints removed our combined model continued to satisfy a great deal of experimental data. This includes the alpha-helical characteristics of the TMD (Fig. 1B) and the appropriate orientation of residues for specific types of labeling experiments. There was excellent fit of the LBD with the TMD (Figs. 1D and 2A and B), despite their completely independent initial construction. Moreover, the model explains experimental data not included in the initial constraints. These include the location of the ion selectivity filter (Fig. 2A), possible sites of anesthetic and alcohol action, and plausible electrostatic interactions between loops in the LBD with the TMD. The latter interactions could be involved in transduction of agonist binding energy in the LBD to structural changes in the TMD. Each of these aspects of our current model serve to explain phenomenon not accounted for by the most recently published coordinates (1OED) of only the TMD in the homologous nAChR [12].

It has become clear that the TMD of the LGICs is composed of a pentamer of tetrameric alpha-helical subunits [16]. While the literature has been quite controversial over the years on this point, the recent model of Miyazawa et al. (1OED.pdb) based on intermediate resolution cryoelectron microscopy electron densities [12] confirms our predictions that were based on secondary structure prediction algorithms. The predicted ends of the TMD alpha helices in our model are in good agreement with those of the 1OED model. However, the position and tilt of the helices in our model show modest differences with those in 1OED (Fig. 1B). These differences can probably be explained by the low resolution of both models and that these channels probably alter their dimensions during the opening and closing processes. In addition, our sequence alignment of residues within the TMD differs somewhat from the positions of homologous residues within the TMD helices of 1OED, as discussed below.

Overall, our sequence alignment and helical arrangement preserved the orientation of residues labeled by hydrophilic and hydrophobic reagents in the TMD. In particular, residues Phe296 and Ser299 in GABAAR, which are TID labeled, hydrophobically accessible residues in TM3 are appropriately positioned in our model but do not face the lipid in 1OED. Furthermore, the packing of TM4 with TM1 and TM3 in our model is quite tight while that in 1OED shows rather large spacing. Such spacing should allow labeling of most TM4 residues with photoaffinity reagents, but that is not the case experimentally [38].

We previously built models of single subunits in the TMD in order to visualize possible binding sites for anesthetics and alcohols [1,8,18,44,45]. Our current model shows a convergence of residues known to be involved in anesthetic and alcohol binding, thereby forming the lining of an anesthetic binding pocket within the core of the tetramer [1]. These include GABAAR Leu232, Ser270, Ala291 and Tyr411. While 1OED displays the appropriate orientation of the residue homologous to Ser267 on TM2, the remaining residues homologous to those known to be involved in anesthetic action are not in proximity.

A region of particular interest is the interface between the LBD and TMD. This region is involved in the transduction of ligand binding information to the TMD. The present model is consistent with the reduced electron density seen at this interface in cryoelectron micrographs of nAChR [22]. This low packing density is appropriate because this region is accessible to methanethiosulfonate reagents, including the TM2–TM3 loop [58,68] and a putative water-filled cavity that includes the extracellular one third of each subunit [45,46]. Reactivity of site-directed cysteine substitutions with methanethiosulfonate reagents in the interfacial region implies that the cysteine thiol groups are ionized and, therefore, that the region is solvated by water [58]. Nevertheless, the coupling between domains is mediated by a peptide link plus vdW and electrostatic interactions between loops 2 and 7 from the LBD and the TM2–TM3 loop in the TMD [7,64]. This coupling is sufficiently strong to convey the energy of agonist binding over 45 A to the gate in the ion pore [2,3].

The mechanism by which the energy of ligand binding at an inter-subunit site can be communicated to the ion channel pore has been the subject of many studies, and this region may be involved in just such an interaction [5,58,69]. Conformational flexibility of the TM2–TM3 loop was recently described in the corresponding loop of the related four-helical bundle of cytochrome b562. A solution NMR structure showed that this loop had the greatest conformational flexibility in the molecule [70]. Such flexibility is important in that ion channel gating involves a rearrangement of individual subunits sufficient to increase access of reagents to a water-filled cavity at the center of the subunit. Although we believe the present model is of the resting state of the channel, it is apparent that an increase in volume of a cavity within a four-helical bundle would occur if the inter-helical crossing angle were increased [71,72].

5. Conclusions

A model of the GABAARa1 built from molluscan, bacterial, and mammalian templates satisfies most experimental criteria for shape, alpha-helical content, exposure of specific residues in labeling experiments, the location of the ion selectivity filter, possible sites of anesthetic and alcohol binding, and the transduction of agonist binding from the LBD to the TMD. This model is also among the first to present atomic level details of an entire LGIC complex containing both LBD and TMD. In the future, many details of the present model will be subject to further refinement. However, the present model will serve as a framework for interpreting ongoing site-directed mutagenesis and labeling studies, and it will allow construction of hypotheses regarding channel function and the effects of anesthetics and alcohols. In addition, it will allow rational selection of appropriate single and multiple site-directed mutations that will be used iteratively to test and refine the model.

Acknowledgement

The research was funded by NIH grants RO1 GM63034 and RO1 AA013378 to JRT, and by the Veterans Administration Health Care System to EB. We wish to thank Dr. Douglas Brutlag for reading the manuscript and Drs. Wayne L. Hubbell, Barry Honig, R. Adron Harris, and Neil Harrison for helpful discussions.

References

[1] T. Yamakura, E. Bertaccini, J.R. Trudell, R.A. Harris, Anesthetics and ion channels: molecular models and sites of anesthetic action, Ann. Rev. Pharmacol. Toxicol. 41 (2001) 23–51.
[2] P.J. Corringer, N. Le Novere, J.P. Changeux, Nicotinic receptors at the amino acid level, Annu. Rev. Pharmacol. Toxicol. 40 (2000) 431–458.
[3] A. Karlin, Emerging structure of the nicotinic acetylcholine receptors, Nat. Rev. Neurosci. 3 (2002) 102–114.
[4] R.W. Olsen, A.J. Tobin, Molecular biology of GABAA receptors, FASEB J. 4 (1990) 1469–1480.
[5] S. Rajendra, J.W. Lynch, P.R. Schofield, The glycine receptor, Pharmacol. Ther. 73 (1997) 121–146.
[6] H.R. Arias, W.R. Kem, J.R. Trudell, M.P. Blanton, Unique general anesthetic binding sites within distinct conformational states of the nicotinic acetylcholine receptor, Int. Rev. Neurobiol. 54 (2003) 1–50.
[7] T.L. Kash, A. Jenkins, J.C. Kelley, J.R. Trudell, N.L. Harrison, Coupling of agonist binding to channel gating in the GABAA receptor, Nature 421 (2003) 421–425.
[8] J.R. Trudell, E. Bertaccini, Molecular modelling of specific and non-specific anaesthetic interactions, Br. J. Anaesth. 89 (2002) 32–40.
[9] M.J. Beckstead, R. Phelan, J.R. Trudell, M.J. Bianchini, S.J. Mihic, Anesthetic and ethanol effects on spontaneously opening glycine receptor channels, J. Neurochem. 82 (2002) 1343–1351.
[10] J.R. Trudell, Unique assignment of inter-subunit association in GABAa alpha1 beta3 gamma2 receptors determined by molecular modeling, Biochim. Biophys. Acta 1565 (2002) 91–96.
[11] K. Brejc, W.J. van Dijk, R.V. Klaassen, M. Schuurmans, O.J. van Der, A.B. Smit, T.K. Sixma, Crystal structure of an ACh-binding protein reveals the ligand-binding domain of nicotinic receptors, Nature 411 (2001) 269–276.
[12] A. Miyazawa, Y. Fujiyoshi, N. Unwin, Structure and gating mechanism of the acetylcholine receptor pore, Nature 424 (2003) 949–955.
[13] S. Yoshikawa, K. Shinzawa-Itoh, R. Nakashima, R. Yaono, E. Yamashita, N. Inoue, M. Yao, M.J. Fei, C.P. Libeu, T. Mizushima, H. Yamaguchi, T. Tomizaki, T. Tsukihara, Redox-coupled crystal structural changes in bovine heart cytochrome c oxidase, Science 280 (1998) 1723–1729.
[14] G. Chang, R.H. Spencer, A.T. Lee, M.T. Barclay, D.C. Rees, Structure of the MscL homolog from mycobacterium tuberculosis: a gated mechanosensitive ion channel, Science 282 (1998) 2220–2226.
[15] M.P. Blanton, J.B. Cohen, Identifying the lipid–protein interface of the torpedo nicotinic acetylcholine receptor: secondary structure implications, Biochemistry 33 (1994) 2859–2872.
[16] E. Bertaccini, J.R. Trudell, Predicting the transmembrane secondary structure of ligand-gated ion channels, Protein Eng. 15 (2002) 443–453.
[17] N. Methot, B.D. Ritchie, M.P. Blanton, J.E. Baenziger, Structure of the pore-forming transmembrane domain of a ligand-gated ion channel, J. Biol. Chem. 276 (2001) 23726–23732.
[18] E. Bertaccini, J.R. Trudell, Molecular modeling of the transmembrane regions of ligand-gated ion channels: progress and challenges, Int. Rev. Neurobiol. 48 (2001) 141–166.
[19] K. Olszewski, L. Yan, D.J. Edwards, SeqFold. Fully automated fold recognition and modeling software. Evaluation and application, Theor. Chem. Acc. 101 (1999) 57–61.
[20] J.F. Gibrat, T. Madej, S.H. Bryant, Surprising similarities in structure comparison, Curr. Opin. Struct. Biol. 6 (1996) 377–385.
[21] N. Unwin, Nicotinic acetylcholine receptor at 9 A resolution, J. Mol. Biol. 229 (1993) 1101–1124.
[22] N. Unwin, A. Miyazawa, J. Li, Y. Fujiyoshi, Activation of the nicotinic acetylcholine receptor involves a switch in conformation of the alpha subunits, J. Mol. Biol. 319 (2002) 1165–1176.
[23] K.A. Huebsch, M.M. Maimone, Rapsyn-mediated clustering of acetylcholine receptor subunits requires the major cytoplasmic loop of the receptor subunits, J. Neurobiol. 54 (2003) 486–501.
[24] M.S.P. Sansom, C. Adcock, G.R. Smith, Modelling and simulation of ion channels: applications to the nicotinic acetylcholine receptor, J. Struct. Biol. 121 (1998) 246–262.
[25] C.E. Capener, H.J. Kim, Y. Arinaminpathy, M.S.P. Sansom, Ion channels: structural bioinformatics and modelling, Hum. Mol. Genet. 11 (2002) 2425–2433.
[26] R.J. Law, D.P. Tieleman, M.S.P. Sansom, Pores formed by the nicotinic receptor m2delta peptide: a molecular dynamics simulation study, Biophys. J. 84 (2003) 14–27.

[27] P. Tang, P.K. Mandal, Y. Xu, NMR structures of the second transmembrane domain of the human glycine receptor alpha(1) subunit: model of pore architecture and channel gating, Biophys. J. 83 (2002) 252–262.
[28] S.J. Opella, F.M. Marassi, J.J. Gesell, A.P. Valente, Y. Kim, M. Oblatt-Montal, M. Montal, Structures of the M2 channel-lining segments from nicotinic acetylcholine and NMDA receptors by NMR spectroscopy, Nat. Struct. Biol. 6 (1999) 374–379.
[29] S. Furois-Corbin, A. Pullman, A possible model for the inner wall of the acetylcholine receptor channel, Biochim. Biophys. Acta 984 (1989) 339–350.
[30] R.H. Spencer, D.C. Rees, The alpha-helix and the organization and gating of channels, Annu. Rev. Biophys. Biomol. Struct. 31 (2002) 207–233.
[31] H.R. Arias, E.A. McCardy, M.J. Gallagher, M.P. Blanton, Interaction of barbiturate analogs with the torpedo californica nicotinic acetylcholine receptor ion channel, Mol. Pharmacol. 60 (2001) 497–506.
[32] H.R. Arias, J.R. Trudell, E.Z. Bayer, B. Hester, E.A. McCardy, M.P. Blanton, Noncompetitive antagonist binding sites in the torpedo nicotinic acetylcholine receptor ion channel. Structure–activity relationship studies using adamantane derivatives, Biochemistry 42 (2003) 7358–7370.
[33] M.H. Akabas, C. Kaufmann, P. Archdeacon, A. Karlin, Identification of acetylcholine receptor channel-lining residues in the entire M2 segment of the a subunit, Neuron 13 (1994) 919–927.
[34] G.G. Wilson, A. Karlin, The location of the gate in the acetylcholine receptor channel, Neuron 20 (1998) 1269–1281.
[35] M.V. Jones, Y. Sahra, J.A. Dzubay, G.L. Westerbrook, Defining affinity with the GABAa receptor, J. Neurosci. 18 (1998) 8590–8604.
[36] A.D. Nagi, K.S. Anderson, L. Regan, Using loop length variants to dissect the folding pathway of a four-helix-bundle protein, J. Mol. Biol. 286 (1999) 257–265.
[37] H.L. Liu, Y.C. Shu, Y.H. Wu, Molecular dynamics simulations to determine the optimal loop length in the helix-loop-helix motif, J. Biomol. Struct. Dyn. 20 (2003) 741–745.
[38] M.P. Blanton, L.J. Dangott, S.K. Raja, A.K. Lala, J.B. Cohen, Probing the structure of the nicotinic acetylcholine receptor ion channel with the uncharged photoactivable compound 2-[3H]diazofluorene, J. Biol. Chem. 273 (1998) 8659–8668.
[39] M.H. Akabas, A. Karlin, Identification of acetylcholine receptor channel-lining residues in the M1 segment of the α-subunit, Biochemistry 34 (1995) 12496–12500.
[40] B.X. Carlson, A.C. Engblom, U. Kristiansen, A. Schousboe, R.W. Olsen, A single glycine residue at the entrance to the first membrane-spanning domain of the gamma-aminobutyric acid type A receptor beta(2) subunit affects allosteric sensitivity to GABA and anesthetics, Mol. Pharmacol. 57 (2000) 474–484.
[41] A. Jenkins, E.P. Greenblatt, H.J. Faulkner, E. Bertaccini, A. Light, A. Lin, A. Andreasen, A. Viner, J.R. Trudell, N.L. Harrison, Evidence for a common binding cavity for three general anesthetics within the GABAA receptor, J. Neurosci. 21 (2001) RC136.
[42] J. Horenstein, D.A. Wagner, C. Czajkowski, M.H. Akabas, Protein mobility and GABA-induced conformational changes in GABA(A) receptor pore-lining M2 segment, Nat. Neurosci. 4 (2001) 477–485.
[43] S.J. Mihic, Q. Ye, M.J. Wick, V.V. Koltchine, M.D. Krasowski, S.E. Finn, M.P. Mascia, C.F. Valenzuela, K.K. Hanson, E.P. Greenblatt, R.A. Harris, N.L. Harrison, Sites of alcohol and volatile anaesthetic action on GABA(A) and glycine receptors, Nature 389 (1997) 385–389.
[44] M.J. Wick, S.J. Mihic, S. Ueno, M.P. Mascia, J.R. Trudell, S.J. Brozowski, Q. Ye, N.L. Harrison, R.A. Harris, Mutations of GABA and glycine receptors change alcohol cutoff: evidence for an alcohol receptor, Proc. Natl. Acad. Sci. U.S.A. 95 (1998) 6504–6509.
[45] M.P. Mascia, J.R. Trudell, R.A. Harris, Specific binding sites for alcohols and anesthetics on ligand-gated ion channels, Proc. Natl. Acad. Sci. U.S.A. 97 (2000) 9305–9310.
[46] D.B. Williams, M.H. Akabas, GABA increases the water-accessibility of M3 membrane-spanning residues in GABA-A receptors, Biophys. J. 77 (1999) 2563–2574.
[47] H.L. Wang, M. Milone, K. Ohno, X.M. Shen, A. Tsujino, A.P. Batocchi, P. Tonali, J. Brengman, A.G. Engel, S.M. Sine, Acetylcholine receptor M3 domain: stereochemical and volume contributions to channel gating, Nat. Neurosci. 2 (1999) 226–233.
[48] O.T. Jones, M. McNamee, Annular and nonannular binding sites for cholesterol associated with the nicotinic acetylcholine receptor, Biochemistry 27 (1988) 2364–2374.
[49] J. Corbin, H.H. Wang, M.P. Blanton, Identifying the cholesterol binding domain in the nicotinic acetylcholine receptor with[125I]-azido-cholesterol, Biochim. Biophys. Acta 1414 (1998) 65–74.
[50] T. Tobimatsu, Y. Fujita, K. Fukuda, K. Tanaka, Y. Mori, T. Konno, M. Mishina, S. Numa, Effects of substitution of putative transmembrane segments on nicotinic acetylcholine receptor function, FEBS Lett. 222 (1987) 56–62.
[51] S. Tamamizu, Y.H. Lee, B. Hung, M. McNamee, J.A. Lasalde-Dominicci, Alteration in ion channel function of mouse nicotinic acetylcholine receptor by mutations in the M4 transmembrane domain, J. Membr. Biol. 170 (1999) 157–164.
[52] A. Jenkins, A. Andreasen, J.R. Trudell, N.L. Harrison, Tryptophan scanning mutagenesis in TM4 of the GABA(A) receptor alpha1 subunit: implications for modulation by inhaled anesthetics and ion channel structure, Neuropharmacology 43 (2002) 669–678.
[53] C. Bouzat, F.J. Barrantes, S.M. Sine, Nicotinic receptor fourth transmembrane domain: hydrogen bonding by conserved threonine contributes to channel gating kinetics, J. Gen. Physiol. 115 (2000) 663–671.
[54] I. Garbus, A.M. Roccamo, F.J. Barrantes, Identification of threonine 422 in transmembrane domain alpha M4 of the nicotinic acetylcholine receptor as a possible site of interaction with hydrocortisone, Neuropharmacology 43 (2002) 65–73.
[55] D. Donnelly, J.P. Overington, T.L. Blundell, The prediction and orientation of alpha-helices from sequence alignments: the combined use of environment-dependent substitution tables, Fourier transform methods and helix capping rules, Protein Eng. 7 (1994) 645–653.
[56] I.D. Kerr, R. Sankararamakrishnan, O.S. Smart, M.S.P. Sansom, Parallel helix bundles and ion channels: molecular modeling via simulated annealing and restrained molecular dynamics, Biophys. J. 67 (1994) 1501–1515.
[57] M. Karplus, J.A. McCammon, Molecular dynamics simulations of biomolecules, Nat. Struct. Biol. 9 (2002) 646–652.
[58] A.K. Bera, M. Chatav, M.H. Akabas, GABAA receptor M2–M3 loop secondary structure and changes in accessibility during channel gating, J. Biol. Chem. 277 (2002) 43002–43010.
[59] M.L. Jensen, D.B. Timmermann, T.H. Johansen, A. Schousboe, T. Varming, P.K. Ahring, The beta subunit determines the ion selectivity of the GABAA receptor, J. Biol. Chem. 277 (2002) 41438–41447.
[60] V.E. Wotring, T.S. Miller, D.S. Weiss, Mutations at the GABA receptor selectivity filter: a possible role for effective charges, J. Physiol. 548 (2003) 527–540.
[61] J.L. Eisele, S. Bertrand, J.L. Galzi, A. Devillers-Thiery, J.P. Changeux, D. Bertrand, Chimaeric nicotinic–serotonergic receptor combines distinct ligand binding and channel specificities, Nature 366 (1993) 479–483.
[62] H. Dang, P.M. England, S.S. Farivar, D.A. Dougherty, H.A. Lester, Probing the role of a conserved M1 proline residue in 5-hydroxytryptamine(3) receptor gating, Mol. Pharmacol. 57 (2000) 1114–1122.
[63] N. Unwin, The Croonian Lecture 2000. Nicotinic acetylcholine receptor and the structural basis of fast synaptic transmission, Phil. Trans. R. Soc. London B Biol. Sci. 355 (2000) 1813–1829.

[64] T.L. Kash, M.J. Dizon, J.R. Trudell, N.L. Harrison, Charged residues in the {beta}2 subunit involved in GABAA receptor activation, J. Biol. Chem. 279 (2004) 4887–4893.
[65] S.M. O'Shea, N.L. Harrison, Arg-274 and Leu-277 of the gamma-aminobutyric acid type A receptor alpha 2 subunit define agonist efficacy and potency, J. Biol. Chem. 275 (2000) 22764–22768.
[66] M.P. Blanton, Y. Xie, L.J. Dangott, J.B. Cohen, The steroid promegestone is a noncompetitive antagonist of the torpedo nicotinic acetylcholine receptor that interacts with the lipid–protein interface, Mol. Pharmacol. 55 (1999) 269–278.
[67] T. Tsukihara, H. Aoyama, E. Yamashita, T. Tomizaki, H. Yamaguchi, K. Shinzawa-Itoh, R. Nakashima, R. Yaono, S. Yoshikawa, The whole structure of the 13-subunit oxidized cytochrome c oxidase at 2.8 A, Science 272 (1996) 1136–1144.
[68] J.W. Lynch, N.L. Han, J. Haddrill, K.D. Pierce, P.R. Schofield, The surface accessibility of the glycine receptor M2–M3 loop is increased in the channel open state, J. Neurosci. 21 (2001) 2589–2599.
[69] C. Grosman, F.N. Salamone, S.M. Sine, A. Auerbach, The extracellular linker of muscle acetylcholine receptor channels is a gating control element, J. Gen. Physiol. 116 (2000) 327–340.
[70] F. Arnesano, L. Banci, I. Bertini, J. Faraone-Mennella, A. Rosato, P.D. Barker, A.R. Fersht, The solution structure of oxidized *Escherichia coli* cytochrome b562, Biochemistry 38 (1999) 8657–8670.
[71] J.U. Bowie, Helix packing angle preferences, Nat. Struct. Biol. 4 (1997) 915–917.
[72] P.C. Weber, F.R. Salemme, Structural and functional diversity in 4-alpha-helical proteins, Nature 287 (1980) 82–84.